Microstructural properties of the Al–Mg_X/TiC composites obtained by infiltration techniques

2004 J. Phys.: Condens. Matter 16 S2241

(http://iopscience.iop.org/0953-8984/16/22/025)

INSTITUTE OF PHYSICS PUBLISHING JOURNAL OF PHYSICS: CONDENSED MATTER

J. Phys.: Condens. Matter **16** (2004) S2241–S2249 PII: S0953-8984(04)76419-X

Microstructural properties of the Al–Mg_x/TiC composites obtained by infiltration techniques

A Contreras[1], **A Albiter and R Pérez**

Instituto Mexicano del Petróleo, Programa de Investigación y Desarrollo de Ductos, Eje Central Lázaro Cárdenas 152, Colonia San Bartolo Atepehuacan, México DF, 07730, Mexico

E-mail: acontrer@imp.mx

Received 16 October 2003
Published 21 May 2004
Online at stacks.iop.org/JPhysCM/16/S2241
DOI: 10.1088/0953-8984/16/22/025

Abstract

Al–Mg_x metal matrix composites reinforced with TiC (56 vol%) were obtained using a pressureless infiltration technique. It was observed that the infiltration rate of these Al–Mg_x alloys increases as the magnesium content increases. Through x-ray diffraction (XRD) no reaction phase was detected, only the presence of aluminium and titanium carbide. In addition, some TEM studies were carried out to characterize the interface and the matrix of the composites. These results suggest that the Mg forms a solid solution with the aluminium lattice. Different morphological and chemical characteristics of the precipitated particles are also reported. To get an insight into the interface phenomena in the HREM images, theoretical simulations have been carried out. The hardness of the Al–Mg_x/TiC composites increases as the amount of magnesium is increased. Additionally, hardness measurements have been performed with an atomic force microscope (AFM) and comparison with steel values were carried out. The elastic modulus, on the other hand, decreases slightly with magnesium content.

(Some figures in this article are in colour only in the electronic version)

1. Introduction

Metal matrix composites (MMCs) reinforced with ceramic particles usually offer good mechanical properties under high temperature conditions [1–3]. The microstructure characteristics of these materials are strongly dependent on the fabrication procedures of the MMCs. In this investigation, pressureless melt infiltration of the ceramic preforms is the technique used in MMC fabrication [4, 5]. Pure aluminium and also aluminium alloys are the most common matrices employed in the metal–ceramic composites. Past investigations [2, 4–7], have shown that additions of TiC as a reinforcement improves the mechanical properties

[1] Author to whom any correspondence should be addressed.

of the MMCs at high temperatures. Pressureless melt infiltration of ceramic preforms is an attractive technique for fabricating metal matrix composites. It allows the production of materials with a high ceramic content without the use of an external force [4]. The nature of the technique used in the fabrication of MMCs has a significant effect on the overall properties of the product. In the case of the liquid–metal processing of composites, a major difficulty is the non-wetting nature of the ceramic reinforcements by liquid metals. Therefore improved wetting must be achieved in order to obtain good bonding between the matrix and the reinforcements [8]. Interfacial properties, and in particular the wetting behaviour, play an important role in the evolution of the microstructure during the processing stages of metal ceramic composites.

In this investigation, the role of magnesium on the infiltration mechanism is explored. Structural and chemical characterizations of the Al–Mg/TiC reinforced composite have been carried out. Transmission electron microscopy (TEM) and x-ray diffraction (XRD) techniques have been the main tools in the characterization process. Some mechanical properties of these composites are also explored.

2. Experimental procedures

The Al–Mg alloys were obtained by melting commercial pure aluminium in a graphite crucible and adding Mg. The compositions of the alloys were 1, 4, 8 and 20 wt% of Mg. Pure commercial aluminium and magnesium were also infiltrated for comparison purposes. The reinforcement material was based on titanium carbide powder with anaverage particle size of 1.2 μm and surface area of 2.32 $m^2\ g^{-1}$. The ceramic preforms of approximately 6.3 cm $\times$ 1 cm $\times$ 1 cm in size, were obtained using an uniaxial press with 18.5 g loads and 8 MPa of pressure in a rectangular die to form the green bars. The sintering process was carried out at 1250 °C in argon atmosphere. Density measurement was performed according to the Archimedes method (ASTM-373), and the percentage of porosity obtained in the preforms was 44%. The infiltration was carried out in a thermo-gravimetric analyser at 900 °C under an argon atmosphere. A full description of the method is described in a previous work [7]. The weight change in the preforms as a result of the infiltration of the liquid (melted) alloy into the TiC preforms was monitored to obtain the infiltration profiles of the samples.

The resulting microstructures and reaction products on the composites were investigated by x-ray diffraction (XRD), scanning electron microscopy (XL-30 ESEM Philips Environment scanning electron microscope), and energy dispersive spectroscopy (EDS) analysis. TEM specimens were prepared initially by electro-polishing techniques and subsequently an ion-beam instrument was used for the final polishing. SEM specimens were obtained just by mechanical polishing. To get an insight into the interface phenomena, theoretical simulations have been carried out. Vickers hardness measurements were carried out using a standard Vickers tester with a 50 kg load. The elastic modulus of the composites was obtained with a Grindosonic–Lemmens instrument and using AFM.

3. Results and discussion

Figure 1 shows the infiltration profiles obtained from the Al–Mg_x binary alloys at 900 °C. The figure shows the infiltration rates of Al–Mg alloys increased with increasing the magnesium contents. The infiltration rates are usually a function of the viscosity and also of the surface tension of the liquid metal. The results from figure 1 indicate that Mg is capable of reducing both properties, leading to an improved motion of the liquid into the porous network, which in turn increases the fluidity of the molten metal [9]. Figure 1 also shows that the infiltration rates for the Al–Mg alloys and for the pure Mg were smaller than for pure aluminium. This

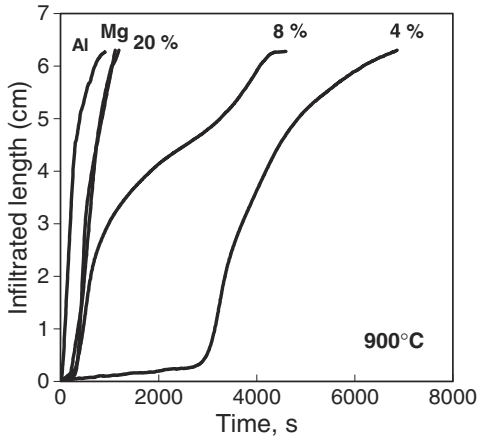

Figure 1. Infiltration profiles of Al–Mg_x/TiC composites obtained at 900 °C.

could be related to the formation of MgO [4, 5]. Therefore, it is possible that the oxidation of Mg affects the infiltration process. Al_2O_3 is thermodynamically stable in contact with pure aluminium melt; however, when the alloys contain magnesium, MgO can be formed:

$$\begin{aligned} &Mg(l) + 1/2O_2(g) = MgO(s) \\ &\Delta G(900\,^{\circ}C) = -473.19\,kJ. \end{aligned} \tag{1}$$

Moreover, thermodynamically MgO is more stable than Al_2O_3. Therefore, Mg can reduce the aluminium oxide according to the reaction:

$$\begin{aligned} &3Mg(l) + Al_2O_3(s) = 3MgO(s) + 2Al(l) \\ &\Delta G(900\,^{\circ}C) = -123.86\,kJ. \end{aligned} \tag{2}$$

If this reaction takes place, Mg tends to form a surface oxide in addition to the Al_2O_3 layer, inhibiting real contact between the TiC and the aluminium. At high magnesium levels and lower temperatures, MgO may form, while the spinel ($MgAl_2O_4$) will form at very low magnesium levels [10–12]. In addition, it is believed that evaporation of Mg can help to disrupt the oxide layer of the melt to allow real contact between TiC and aluminium [13, 14]. This phenomenon was present during infiltration, since powdered Mg was found on the inner surface of the tube after every experiment, even though Mg has a boiling point near to 1120 °C and the experiments were carried out in a dynamic atmosphere of argon. An XRD analysis of these powders revealed the formation of MgO. There is an incubation period prior to stabilization into parabolic type infiltration curves. This period is more noticeable for Al–4Mg alloy and becomes less significant as the infiltration temperature and magnesium increases.

Figure 2 shows the typical microstructure of the as-infiltrated Al–Mg_x/TiC composites. The dark phase is the aluminium matrix and the white bright phase is related to the TiC grains. Total infiltration was obtained with the Al–Mg_x alloys and also with the pure Mg and pure Al. The SEM micrographs show that the earlier porous network was occupied by the aluminium alloys, forming a continuous interconnected metal matrix. Magnesium does not form stable carbides; therefore the TiC is a suitable reinforcement for the Al–Mg matrix composites.

Figure 3 shows the x-ray diffraction patterns obtained from the different composites. This figure illustrates similar crystalline characteristics of the different metal matrix composites fabricated. These results suggest that the matrix and the ceramic do not experience any interfacial reaction. TEM observations have also been carried out on some obtained

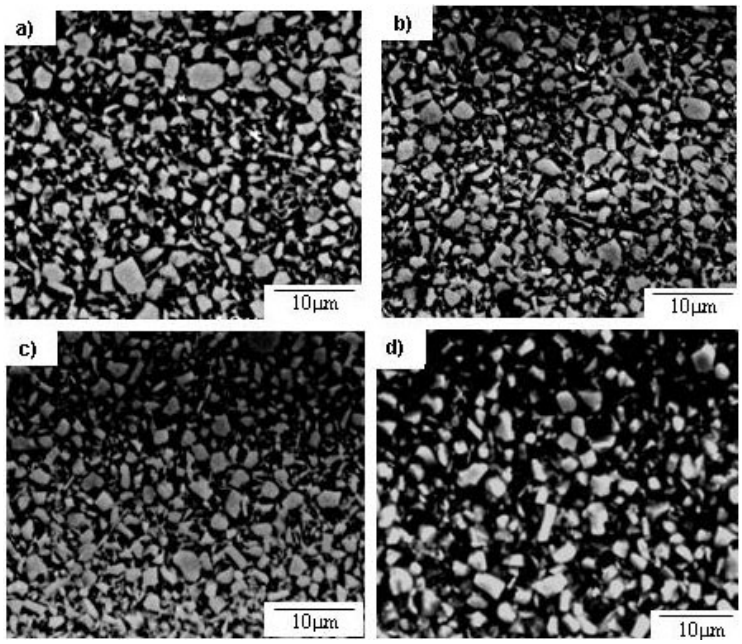

Figure 2. SEM images of: (a) Al–1Mg/TiC, (b) Al–4Mg/TiC, (c) Al–8Mg/TiC and (d) Al–20Mg/TiC composites, infiltrated at 900 °C.

composites. Figure 4 shows the bright and dark field images of a typical Al–4Mg/TiC specimen. Both images show high density of nanometric precipitated particles ($\leqslant$20 nm), embedded in the alloyed matrix. There are also larger size precipitated particles. Thus, for example, figure 5 shows three different specimen regions (1, 2 and 3) where different particles can be seen. The image shows precipitates of different size and morphology. Chemical analysis suggest that particle 3 (bright contrast) corresponds to a titanium carbide particle. However, regions 1 and 2 show complex compositional stoichiometries. This is illustrated in figure 5 (1 and 2), where a TiC stoichiometry and signals from Al, O and Mg can clearly be seen.

Past investigations [10] on the magnesium additions has led to spinel formation along the metal/ceramic interface. In this study, no spinel formation was detected with the XRD technique. However, line scans and point microanalysis (EDS) were obtained from the Al–20Mg/TiC, the results suggest stoichiometries closely related to spinel formation ($MgAl_2O_4$) and $MgAlO_2$ and Mg_2AlO_3.

Figure 6 shows the bright and dark field images of a specimen obtained from the Al–20Mg/TiC composite. The dark field image shows small ($\sim$2–3 nm) precipitated particles. The EDS spectra indicate a titanium carbide region (figure 6(c)). HREM images of this region have also been obtained. Figure 7 shows the image obtained from this region. It is interesting to point out that the HREM image does not show the clear presence of the precipitated nanometric particles. This image shows a lattice fringe square arrangement with regions of different bright dot intensities. One interesting feature of this HREM image is the square bright regions which show dislocations in the square corners, this is illustrated in figure 7. The image resembles the presence of a small square particle embedded in the matrix with dislocations in the stressed areas. To get an insight into the interface phenomena in the HREM image, theoretical simulations have been carried out. The main goal of this simulation is to clarify the interface phenomena appearing in our TEM image. Based on this idea, a small

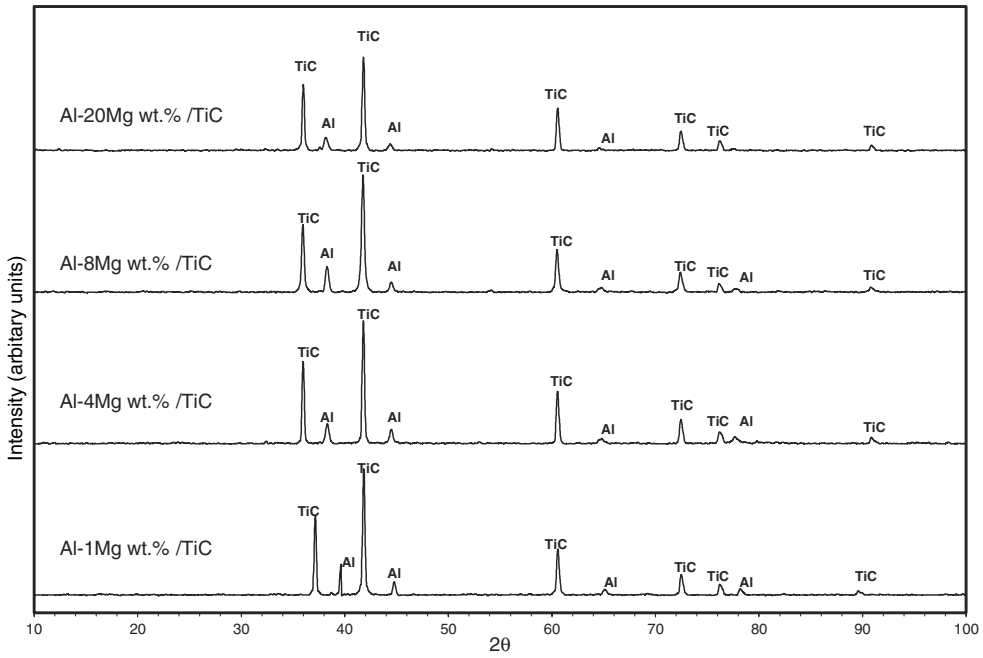

Figure 3. X-ray diffractograms from Al–Mg$_x$/TiC composites infiltrated at 900 °C.

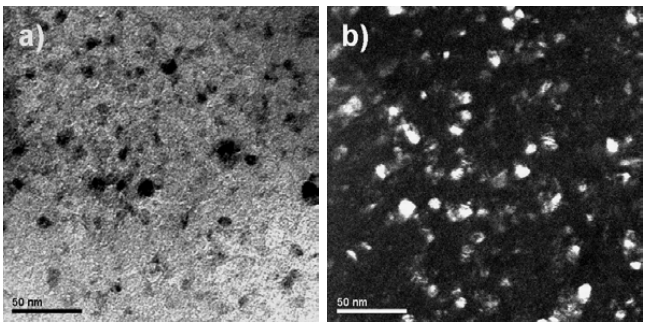

Figure 4. (a) Bright and (b) dark field images of nanometric particles embedded in the alloyed matrix (Al–4Mg/TiC composite).

cubic rutile TiO_2 (because the lattice parameter is in accordance with TiO_2: 2.25 Å) crystal was constructed and embedded in the hole of a bulk TiC crystal (figure 8(a)). Meanwhile, in order to avoid the image force of the embedding rutile TiO_2 crystallite and surface effect on interface of two crystals, the size of the whole system was adequately large and exerted free surface conditions instead of periodic boundary conditions. Their separation is large enough to ensure freedom in the degree of relaxation. The relaxed configuration shows that the multiple defects are produced by the embedding cluster. This result can more clearly be seen from the simulated HREM image (figure 8(b)). In this figure the deformed regions on the particle corners can be seen. This result qualitatively resembles the image contrast illustrated in figure 7. The interatomic potentials for pure metals used in this work are from Ruda *et al* [15] for C, from Pasianot [16] for Ti, and from Voter and Chen [17, 18] for Al. The interatomic potentials for

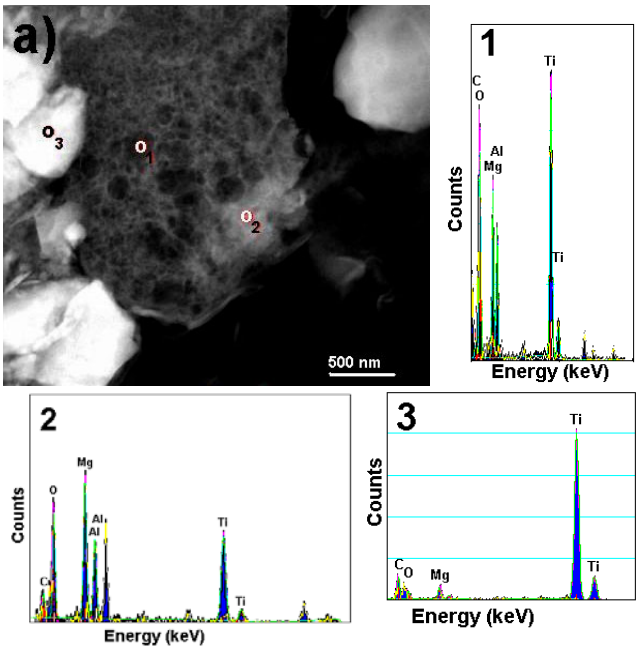

Figure 5. (a) TEM image obtained from the Al–4Mg/TiC composite. (1), (2) and (3) EDS spectra from three different regions.

Table 1. Hardness and elastic modulus of Al–Mg_x/TiC composites.

System	Hardness (Vickers)	Elastic modulus (GPa)
Al–1Mg/TiC	262.2	170.5
Al–4Mg/TiC	285.3	164.3
Al–8Mg/TiC	315.1	160
Al–20Mg/TiC	340.0	150.5
Al/TiC	223	170
Mg/TiC	187	129.5

unlike atoms used in this work are from Farkas *et al* [19] for Ti–Al, from Ruda *et al* [15] for Ti–C and Al–C.

Finally, Vickers hardness measurements of the composites have been obtained. These measurements were carried out using a standard Vickers tester with a 50 kg load and also using AFM. Table 1 shows the hardness and the elastic modulus of the Al–Mg_x/TiC composites. The hardness increases as the amount of Mg is increased. The maximum value is obtained at 340 HV, which corresponds to the Al–20Mg/TiC composite. However, the pure Mg/TiC and pure Al/TiC composites present hardness values of 187 and 223 HV respectively. The elastic modulus of the preforms before infiltration was of the order of 30–35 GPa. The elastic modulus of the AlMg_x/TiC samples decreased slightly with the increase of Mg content in the alloys, which is in agreement with that reported for AlMg binary alloys [20]. Thus the elastic modulus of the pure Al/TiC composite (170 GPa) decreased by alloying with Mg until it reached 129.5 GPa for the pure Mg/TiC composite. Nanohardness measurements have been obtained using an AFM. Nanohardness values were obtained from different specimens and

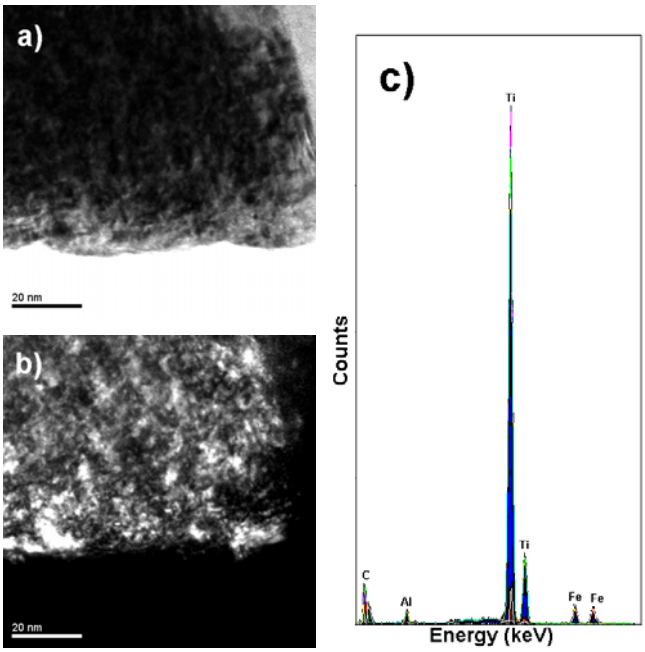

Figure 6. (a) Bright and (b) dark field images showing nanometric particles, (c) EDS spectrum from the region illustrated in (a) and (b). The spectrum shows a titanium carbide region.

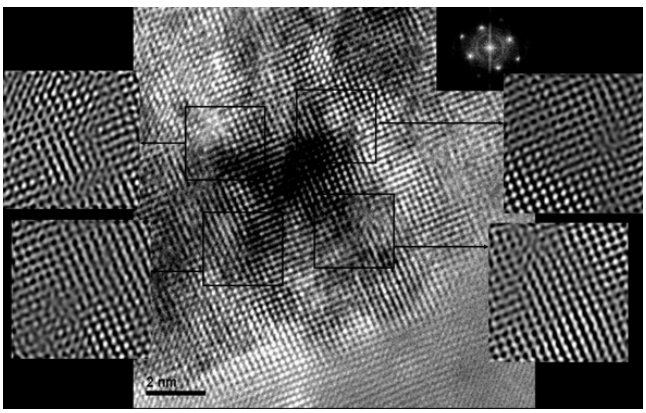

Figure 7. HREM image obtained from the edge of the specimen shown in figures 6(a) and (b). Square regions show dislocations in their corners.

in different sites. Table 2 shows the obtained values. This table indicates that some of the obtained composites have hardness values comparable to X-52 steel, and even higher values.

4. Conclusions

AlMg$_x$/TiC composites were fabricated using the pressureless infiltration technique. It was observed the infiltration rates increased with the increase of the magnesium in the Al–Mg$_x$ alloys. It was found that pure aluminium infiltrated faster than pure Mg, whereas oxidation

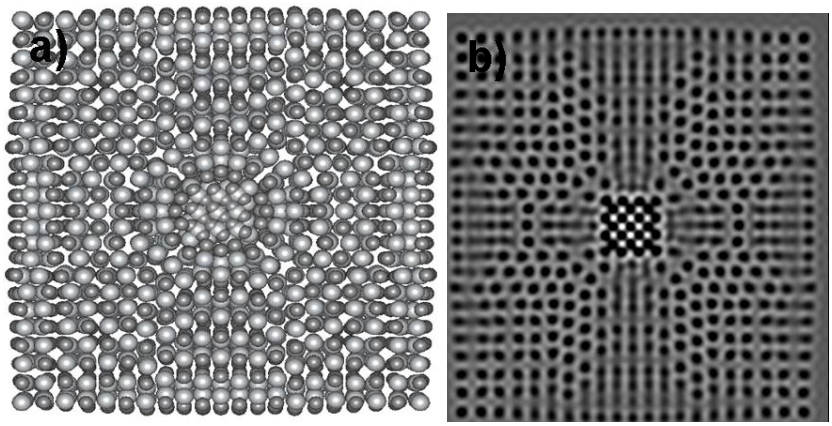

Figure 8. (a) Atomic model of a small cubic rutile (TiO_2) crystal constructed and embedded in the hole of a bulk TiC crystal. (b) Theoretical HREM image based on the atomic model displayed in (a).

Table 2. Nanohardness measurements from Al–Mg_x/TiC composites using AFM.

System	Region	Applied force f (kg)	Hardness (Vickers)
Al–4Mg/TiC	1	9.10E−07	62.79
Al–20Mg/TiC	1	1.72E−06	119.02
Al–4Mg/TiC	2	9.28E−07	64.03
Al–20Mg/TiC	2	1.64E−06	113.16
X–52 steel	X	1.41E−06	97.80

of Mg led to a slower infiltration rate of AlMg-alloys. The x-ray diffraction patterns of all the composites show similar crystalline phases. There are no interface reactions between the matrix and the ceramic reinforcement detected through x-ray diffraction. Different grain sizes are obtained, sizes range from nanometric particles up to micrometre sizes. Some of the particles are of the TiC and also TiO_2 nature. The results of the theoretical simulations show that the multiples defects are produced by the embedding cluster. The composite hardness increases as the Mg content is increased. Its magnitude is larger than the Al and Mg matrix composites. The elastic modulus of the Al–Mg_x/TiC is lower than the Al/TiC but higher than the Mg/TiC composites.

Acknowledgments

The authors are grateful for the experimental support received from Instituto de Investigaciones Metalúrgicas, from Universidad Michoacana, México. Also, they would like to acknowledge Dr J Ascencio and Dr H Bo Liu for their help with the theoretical simulations.

References

[1] Taha M A 2001 *Mater. Des.* **22** 431
[2] Muscat D and Drew R A L 1994 *Metall. Mater. Trans.* A **25** 2357
[3] López V H, Scoles A and Kennedy A R 2003 *Mater. Sci. Eng.* A **356** 316

[4] Contreras A, León C A, Drew R A L and Bedolla E 2001 Design, manufacturing and application of composites *CANCOM-2001* ed S V Hoa, A Johnston and J Denault p 453
[5] Contreras A, Albiter A, Bedolla E and Pérez R 2003 *Composites* A submitted
[6] Albiter A, León C A, Drew R A L and Bedolla E 2000 *Mater. Sci. Eng.* A **289** 109
[7] Contreras A, Salazar M, León C A, Drew R A L and Bedolla E 2000 *Mater. Manuf. Process.* **15** 163
[8] Contreras A, León C A, Drew R A L and Bedolla E 2003 *Scr. Mater.* 1625
[9] Goicochea J C, Garcia Cordovilla E, Louis E and Palies A 1992 *J. Mater. Sci.* **27** 5247
[10] Lloyd D J 1994 *Int. Mater. Rev.* **39** 1
[11] Pai B C, Ramani G, Pillai R M and Satyanarayana K G 1995 *J. Mater. Sci.* **30** 1903
[12] McLeod A D and Gabryel C M 1992 *Metall. Trans.* A **23** 1279
[13] Lopez V H, Truelove S and Kennedy A R 2003 *Mater. Sci. Technol.* **19** 1
[14] León C A, Lopez V H, Bedolla E and Drew R A L 2002 *J. Mater. Sci.* **37** 3509
[15] Ruda M, Farkas D and Abriata J 2002 *Scr. Mater.* **46** 349
[16] Pasianot R and Savino E J 1992 *Phys. Rev.* B **45** 12704
[17] Voter A F and Chen S P 1987 *Mater. Res. Soc. Symp. Proc.* **82** 175
[18] Voter A F 1995 *Intermetallic Compounds: Principles and Practice* vol 1, ed J H Westbrook and R L Fleischer (New York: Wiley) p 77
[19] Farkas D 1994 *Mater. Sci. Eng.* **2** 975
[20] Hatch J E 1984 *Aluminum: Properties and Physical Metallurgy* (Metals Park, OH: ASM International)